Wu et al. Nanoscale Research Letters (2017) 12:85
DOI 10.1186/s11671-017-1867-5

Nanoscale Research Letters

NANO EXPRESS Open Access

Balanced Dipole Effects on Interfacial Engineering for Polymer/TiO_2 Array Hybrid Solar Cells

Fan Wu[1*], Yanyan Zhu[1], Xunheng Ye[1], Xiaoyi Li[1], Yanhua Tong[2] and Jiaxing Xu[1]

Abstract

The polymer/TiO_2 array heterojunction interfacial characteristics can be tailored by balanced dipole effects through integration of TiO_2-quantum dots (QDs) and N719 at heterojunction interface, resulting in the tunable photovoltaic performance. The changes of V_{oc} with interfacial engineering originate from the shift of the conduction band (E_c) edge in the TiO_2 nanorod by the interfacial dipole with different directions (directed away or toward the TiO_2 nanorod). The J_{sc} improvement originates from the enhanced charge separation efficiency with an improved electronic coupling property and better charge transfer property. The balanced dipole effects caused by TiO_2-QDs and N719 modification on the device V_{oc} are confirmed by the changed built-in voltage V_{bi} and reverse saturation current density J_s.

Keywords: TiO_2, Array, Hybrid solar cells, Interfacial engineering

Background

TiO_2 is mainly used in photocatalytic and photoelectrode for photocurrent because of its nontoxicity, high electron mobility, and high chemical and thermal stability [1, 2]. Hybrid solar cells (HSCs) based on conjugated conducting polymers (donor) and TiO_2 nanocrystals (acceptor) have received extensive attention, as they have the potential to offer low-cost, mechanically flexible, and up-scalable alternatives to conventional photovoltaics [3, 4]. A promising photovoltaic device structure for HSC consisting of a direct and ordered path, instead of disordered three-dimensional networks of interconnected nanoparticles for electron transport to the collecting electrode, has been proposed [5, 6]. Single-crystalline rutile TiO_2 nanorod arrays (NRAs) are hydrothermally grown directly on fluorine-doped tin oxide (FTO) substrates as acceptors to dissociate excitons and collect electrons in a HSC, which demonstrates an enhanced power conversion efficiency compared with that of the dense TiO_2 film-based device [7, 8]. However, in general, the polymer/pristine TiO_2-NRA solar cells perform poorly, wherein most of the open-circuit voltage (V_{oc}) is 0.30–0.44 V and the short-circuit current (J_{sc}) is between 0.28–2.20 mA/cm^2 [7–10]. It was demonstrated that the interfaces between the polymer and the nanocrystals play a crucial role in determining the photovoltaic performance. The relatively poor performance of the polymer/pristine TiO_2-NRA solar cells can be partly attributed to the undesirable interfacial properties between the polymer and TiO_2-NRAs [11, 12].

Optimization of the polymer/nanocrystal interface can enhance the charge separation efficiency and reduce the charge recombination and is an important issue for efficient HSC devices [13]. Therefore, to improve device performance, various studies have been performed on modified TiO_2-NRA surfaces. For example, TiO_2-NRA modified with an organic molecule (i.e., D149) has improved the J_{sc} to 3.93 mA/cm^2 and V_{oc} to 0.60 V due to the improved compatibility of the interface morphology [11]; inorganic modification of TiO_2-NRA, such as with crystalline CdS-quantum dots (QDs), normally results in an increase in J_{sc} to 1.51 mA/cm^2 and V_{oc} of 0.45 V [7]; and modification with crystalline CdSe-QDs normally results in an increase in J_{sc} to 1.15 mA/cm^2 and V_{oc} of 0.62 V [14]. It is obvious that both the organic and inorganic modifications differentially affect the polymer/TiO_2-NRA devices' performance. At present, few studies on interfacial engineering of combinations of the organic

* Correspondence: wufanjay@126.com
[1]School of Science and Key Lab of Optoelectronic Materials and Devices, Huzhou University, Huzhou 313000, People's Republic of China
Full list of author information is available at the end of the article

and inorganic material in the polymer/TiO_2-NRA HSCs have been reported. Zhang et al. studied the composite interfacial modification in the P3HT/TiO_2-NRA interface using inorganic (CdSe) and organic (N719 dye, pyridine) materials as modifiers [15]. At present, there are some limitations to improve the device performance by the method of monomodification, which leads to the moderate improvement in device efficiency. In their results, the performance of composite interfacial modification was superior to that of modifications based on a monolayer. Obviously, engineering the heterojunction interface using organic and inorganic materials simultaneously in polymer/TiO_2-NRA HSCs is a method for further improving the photovoltaic performance.

This work aims at the heterojunction interface of polymer/TiO_2-NRA HSCs, two functional materials of TiO_2-QDs and N719 dyes are constructed at the interface of polymer/TiO_2-NRA with certain principles as depicted in Fig. 1, which generates the synergistic effects on device performance. Results showed that the efficiency in our polymer/TiO_2-NRA solar cells can be improved nearly fourfold by engineering the heterojunction interface. Moreover, the photovoltaic performance can be tailored through different amounts of TiO_2-QDs and N719 at heterojunction interface, resulting in the tunable photovoltaic performance.

Methods

Synthesis of TiO_2-NRA

TiO_2-NRA was hydrothermally grown on FTO-coated glass (14 Ω/sq, 400 nm FTO thickness, Nippon Sheet Glass Co.) according to the reported procedure [16]. Deionized water (30 mL) was mixed with 30 mL of concentrated hydrochloric acid (35%) to reach a total volume of 60 mL in a Teflon-lined stainless steel autoclave (100 mL volume). The mixture was stirred in ambient conditions for 5 min, the cleaned FTO substrate was put upside down in the Teflon liner, and 1 mL of titanium (IV) isopropoxide was added. After 10 min of ultrasonic solving, the autoclave was sealed and autoclaving was conducted at 180 °C for 2 h in an electric oven to produce TiO_2-NRA.

Synthesis of TiO_2-NRA@TiO_2-QDs

The TiO_2-NRA substrate was removed, rinsed extensively with deionized water, and dried under airflow. Subsequently, the TiO_2-NRA substrate was put upside down in the Teflon liner and added 0.1 M titanium isopropoxide ethanol solution. The sealed autoclave was heated to 200 °C in an electric oven for another 4 h to produce TiO_2-CSA. Once it cooled, the substrate was removed and dried under airflow after carefully rinsing it with anhydrous alcohol several times.

Synthesis of TiO_2-NRA@TiO_2-QDs@N719

The dried TiO_2-NRA@TiO_2-QD substrate was immersed in ethanol solution of N719 (5×10^{-6} M) in an autoclave and heated to 80 °C for 8 h in an electric oven. After the autoclave was cooled to room temperature, the substrate was removed and rinsed with alcohol several times to remove the excess dye, providing the sample TiO_2-NRA@TiO_2-QDs@N719.

Device Fabrication

The procedure used for fabrication of solar cells was similar to that described in previous works [17, 18]. Poly[2-methoxy-5-(2'-ethylhexyloxy)-p-phenylene vinylene] (MEH-PPV) (average Mn = 40000 – 70000, Aldrich) and poly(3,4-ethylene dioxythiophene):poly(styrene-sulfonate) (PEDOT:PSS) (Clevios P HC V4, H. C. Starck) were commercially obtained. The MEH-PPV layer was deposited on the top of the array by spin-coating (1500 rpm, 40 s) the MEH-PPV solution in chlorobenzene (10 mg/mL) under ambient conditions. Active layer deposition was followed by annealing at 150 °C under N_2 atmosphere for 10 min. Subsequently, a PEDOT:PSS film was spin coated (2000 rpm, 60 s) over the polymer layer. After the deposition of PEDOT:PSS, the sample was sequentially heated for 10 min at 100 °C in a N2 glove box. Finally, a gold electrode (100 nm) was evaporated through a shadow mask to form an overlapped area of 3 mm × 3 mm between the indium tin oxide (ITO) and Au, which was defined as the effective device area.

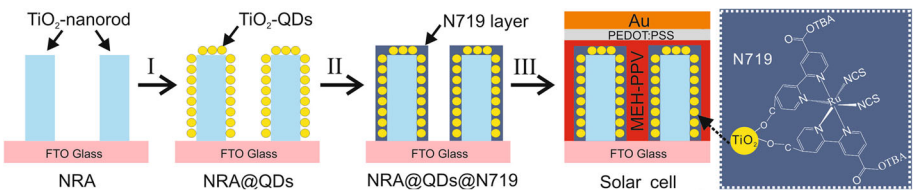

Fig. 1 Schematic illustration for the interfacial engineering in a polymer/TiO_2-NRA solar cell by a combination of TiO_2-QDs and organic molecules N719 and the architecture of solar cells

Characterizations and Measurements

Scanning electron microscopy (SEM) measurements of nanostructures were performed with field-emission scanning electron microscopy (FE-SEM, Hitachi S-4700). Transmission electron microscopy (TEM) and high-resolution TEM (HRTEM) studies were performed on a JEOL-2010 microscope under an acceleration voltage of 200 kV. The room temperature photoluminescence (PL) properties were measured in ambient conditions. PL measurements were made with a Hitachi F-7000 spectrofluorophotometer. The steady-state J–V curves were measured with AM 1.5 illumination under ambient conditions using a 94023A Oriel Sol3A solar simulator (Newport Stratford, Inc.) with a 450 W xenon lamp as the light source. Incident photon-to-current efficiency (IPCE) spectra of the solar cells were measured by using a QE/IPCE measurement kit (Zolix Instruments Co., Ltd.) in the spectral range of 300 – 900 nm.

Results and Discussion

Figure 2a shows a typical side view of the SEM image of an as-synthesized TiO_2-NRA. The rods stand almost perpendicular to the substrate, have a similar diameter in the 40 to 50 nm range, and are about 500-nm long.

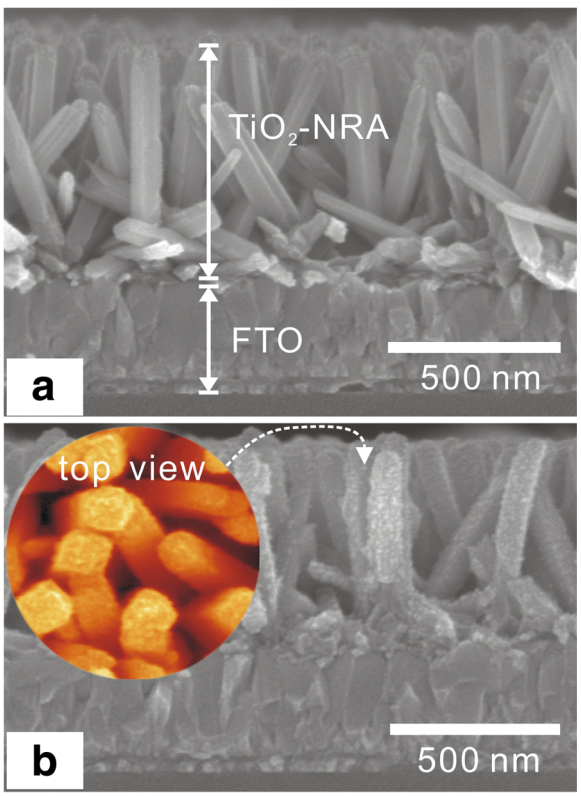

Fig. 2 a and **b** are side views of the SEM images of TiO_2-NRA@TiO_2-QDs on the FTO substrate. The *inset* in (**b**) with pseudocolor is the top view of the TiO_2-NRA@TiO_2-QDs structure

The TiO_2 nanorods in the array are quite smooth surfaces. The SEM image of the TiO_2-NRA after growth of TiO_2-QDs (TiO_2-NRA@TiO_2-QDs) is presented in Fig. 2b. Compared to bare TiO_2-NRA, obvious rough grains eventually spanning the entire nanorod can be observed in the side view and top view. The XRD pattern of the NRA@QD sample (Additional file 1: Figure S1) was only indexed to TiO_2, which confirms that the rough grains are TiO_2. Figure 3 shows a typical TEM image of a sample of TiO_2-NRA and TiO_2-NRA@TiO_2-QDs. The TiO_2 nanorod was single crystalline with quite a smooth surface (Fig. 3a). The lattice fringes with interplanar spacings of 0.29 and 0.32 nm match the crystal planes (001) and (110) of rutile TiO_2, respectively (Fig. 3b) [16]. Figure 3c shows a typical TEM image of a single rod from the TiO_2-NRA@TiO_2-QDs. The coarse surface clearly shows that the TiO_2 nanorod is covered by a TiO_2-QD layer. Figure 3d is a HRTEM image of the rectangular area in Fig. 3c. The shell contains differently oriented TiO_2-QDs with 3 – 5 nm grain sizes. The TiO_2-NRA@TiO_2-QD structures after bonding with $(Bu_4N)_2(Ru)(dcbpyH)_2(NCS)_2$ (called N719) organic molecules were characterized by the absorption spectra and the FT-IR (Additional file 1: Figure S2, in the Supplementary data), which suggest that N719 molecules are chemically grafted onto the TiO_2 surface.

HSCs based on TiO_2-NRA, TiO_2-NRA@TiO_2-QDs, and TiO_2-NRA@TiO_2-QDs@N719 with the conjugated polymer MEH-PPV were fabricated, the architecture of the device is shown in Fig. 1. The illuminated J–V curves (Fig. 4) were measured under the AM 1.5 illumination of 100 mW/cm^2 and the photovoltaic parameters were extracted in the Table 1. The MEH-PPV/TiO_2-NRA device exhibits a rather low V_{oc} (0.314 V), J_{sc} (2.048 mA/cm^2), and efficiency (0.236%) [7–12]. In contrast, after the 4-h growth of the TiO_2-QDs on TiO_2-NRA to form the NRA@QD structure, the V_{oc} are significantly improved, accompanying little improvement in J_{sc}. Further increasing the growth time of TiO_2-QDs will lead to a very slight increase in V_{oc}, but the J_{sc} decreased because the decreased amount of polymer infiltrated into nanorod interspaces [17, 18]. After modifying the TiO_2-NRA@TiO_2-QDs (4 h) with N719 by an 4-h solvothermal reaction, a higher J_{sc} of 3.233 mA/cm^2 was obtained, which is 2–3-fold higher than that of the MEH-PPV/pristine TiO_2-NRA counterpart device; however, the V_{oc} decreased slightly. The power conversion efficiency was enhanced from 0.236 to 0.911%. We also took the N719 reaction time of 8 h to modify the TiO_2-NRA@TiO_2-QD sample. It was found that the V_{oc} was further decreased, but the J_{sc} (4.222 mA/cm^2) was further improved over the sample with the 4-h reaction time. The devices also showed the good stability (Additional file 1: Figure S3, in the Supplementary data). These results suggest that V_{oc} and

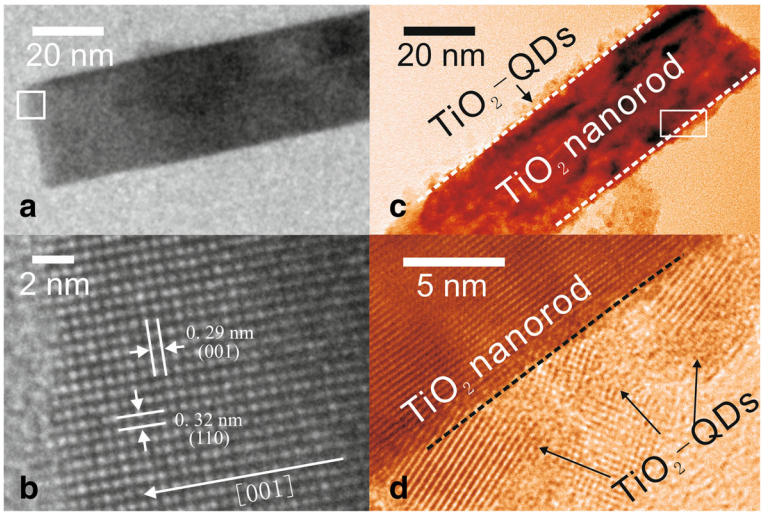

Fig. 3 TEM (**a**, **c**) and HRTEM (**b**, **d**) images of TiO_2-NRA (**a**, **b**) and TiO_2-NRA@TiO_2-QDs. The images of TiO_2-NRA@TiO_2-QDs (**c**, **d**) were processed with pseudocolor to distinguish them from TiO_2-NRA (**a**, **b**). The HRTEM image (**d**) was taken from the white frame on the corresponding TEM images (**c**)

J_{sc} in polymer/TiO_2-NRA solar cells can be tuned by engineering their heterojunction interface with the integration of inorganic and organic materials. The mechanism in detail of above phenomenon will be discussed as follows.

It is well known that V_{oc} in the polymer/inorganic solar cells is mainly determined by the energy levels of the E_c edge in the inorganic material and highest occupied molecular orbital (E_{HOMO}) band in the polymer (Fig. 5a) [6, 19]. The larger V_{oc} in the device with TiO_2-NRA@-TiO_2-QDs than in the device with pristine TiO_2-NRA has been demonstrated from the generation of interfacial dipoles in QD shell/polymer interfaces [17, 18]. The interfacial dipole generation can be considered as the formation of weakly bound pairs of electrons and holes with separations of a few nanometers by Coulombic attraction [20]. These interfacial dipoles commonly arise due to the trapping of electrons at surface states in TiO_2-QD shell with a negative charge at the metal oxide surface and positive charge at the polymer (Fig. 5b) [19]. The E_c of the TiO_2 nanorod can be changed by $e\delta E$ with the presence of interfacial dipoles as is similar to the interfacial modification with dipole molecules in P3HT/TiO_2 [21] and P3HT/ZnO solar cells [22], in which δE is the change of the surface potential and can be calculated from Poisson's equation [23],

$$\delta E = N\mu\cos\theta/\varepsilon_r\varepsilon_0 \quad (1)$$

where N is the dipole concentration, μ the dipole moment, θ the angle the dipole makes to the TiO_2 nanorod surface normal, ε_r the dielectric constant of TiO_2, and ε_0 the permittivity of free space. If dipoles are directed away from the TiO_2 nanorod, $\cos\theta > 0$ and leading to $\delta E > 0$; if dipoles are directed toward the TiO_2 nanorod, $\cos\theta < 0$, leading to $\delta E < 0$. Therefore, the magnitude of E_c shifting correlates with the dipole concentration and direction in the shell/polymer interface. With the

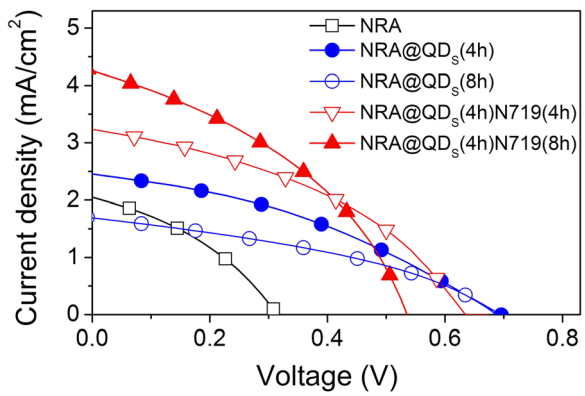

Fig. 4 *J–V* curves of HSCs under the AM 1.5 illumination of 100 mWcm^{-2}

Table 1 Photovoltaic parameters of solar cells under the AM 1.5 illumination of 100 mWcm^{-2}

	V_{oc} (V)	J_{sc} (mA/cm^2)	FF (%)	η (%)
NRA	0.314	2.048	36.740	0.236
NRA@QDs (4 h)	0.695	2.450	36.218	0.616
NRA@QDs (8 h)	0.705	1.680	37.308	0.441
NRA@QDs (4 h)@N719 (4 h)	0.630	3.233	40.980	0.834
NRA@QDs (4 h)@N719 (8 h)	0.540	4.222	39.956	0.911

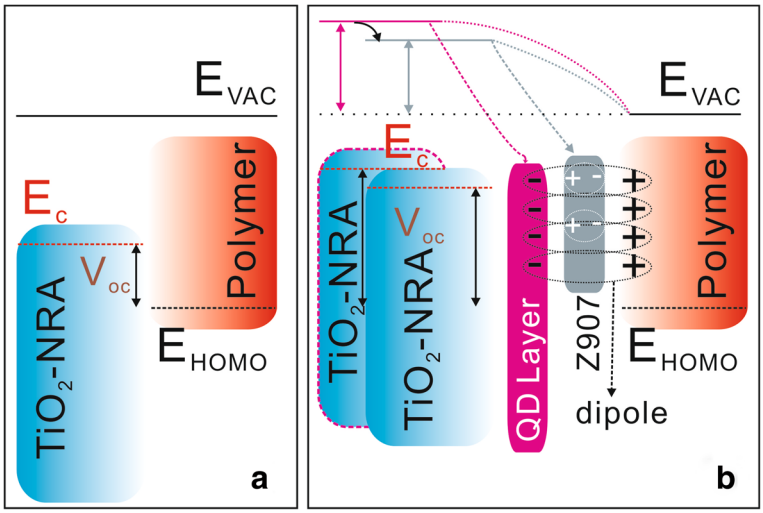

Fig. 5 Polymer/TiO_2-NRA band diagram (**a**) and the band structure changes subjected to interfacial engineering (**b**). E_{vac}, E_c, and E_{HOMO} indicate vacuum, conduction band of TiO_2, and the highest occupied molecular orbital of the polymer energy level, respectively

presence of dipoles directed away from the TiO_2 in the shell/polymer interface (i.e., $\cos\theta > 0$) due to the TiO_2-QD shell (Fig. 8b), the E_c of the TiO_2 nanorod core will be shifted toward the local vacuum level of the polymer due to the $\delta E > 0$ (Fig. 5b).

The obtained V_{oc} of 0.54 and 0.63 V for the MEH-PPV/TiO_2-NRA@TiO_2-QDs&N719-based device, however, are somewhat lower than the value of 0.69 V for the MEH-PPV/TiO_2-NRA@TiO_2-QD-based counterpart device. This results from the modification of the ZnO surface by N719, stemming from the dissociative adsorption of the carboxylic acid group to form a carboxylate bond, in which the positive proton charge on the surface and the negative charge on the carboxylic group together form an interfacial dipole [21, 22]. A theoretical calculation has demonstrated the direction of the dipoles generated by the adsorbed N719 molecules on the oxide surface with the monodentate anchoring mode directed to the oxide surface (i.e., $\cos\theta < 0$) (Fig. 5b) [22]. In this case, the dipole concentration generated by the modification with N719 will change the E_c of the TiO_2 nanorod with $\delta E < 0$ based on eq. (1). That means the V_{oc} will be reduced by shifting the band edge potential of TiO_2 closer to the polymer E_{vac} [20, 24]. The V_{oc} in the MEH-PPV/TiO_2-NRA@TiO_2-QDs&N719 device with 8 h of N719 bonding time was further confirmed in this conclusion (Fig. 2 and Table 1). The dipole concentration in the sample MEH-PPV/TiO_2-NRA@TiO_2-QDs&N719 with 4 h of N719 bonding time should be lower than the counterpart with 8 h. The magnitude of suppressed band edge shifting of TiO_2 (i.e., $\delta E < 0$) should be smaller than the 8-h sample based on eq. (1), which causes the V_{oc} in the 8-h device MEH-PPV/TiO_2-NRA@TiO_2-QDs&N719 to be lower than MEH-PPV/TiO_2-NRA@TiO_2-QD&N719 with 4 h. Therefore, there is a balance of dipole effects (i.e., positive or negative of δE and its magnitude) by QD layer and N719 modification on device V_{oc}.

In addition, the interfacial dipoles were confirmed by the changed built-in voltage V_{bi} (Fig. 6) and reverse current J_s (Fig. 7). The V_{bi} related to built-in electric field (E_{bi}) which originates the work-function difference between the ITO and Au electrodes could be observed at the point where the dark J–V curve begins to follow quadratic behavior [25]. The interfacial dipoles (directed toward the polymer) could induce an extra polar electric field to enhance E_{bi}, which is confirmed by the enhanced V_{bi} in Fig. 6a [22, 23]. Moreover, the E_c edge shifts in the TiO_2 nanorod due to the number of dipole formations also agree with the changes of the reverse saturation current density J_s in the devices, which aroused our much interest. It has been demonstrated that there is often an interface activation energy barrier Φ_B at the heterojunction, which is usually explained as a result of the energy level bending by the vacuum level misalignments at the heterojunction, and could be affected by formation of interface charge transfer state or dipoles [26, 27]; the Φ_B can be evaluated from the dark reverse saturation current in dark J–V characteristic by [40.41]

$$J_s = A \exp\left(-\frac{\Phi_B}{nkT}\right) \tag{2}$$

where A is a coefficient with a value in the vicinity of 1000 A/cm^2 for the reverse bias current generation, and k and T are the Boltzmann constant and temperature, respectively.

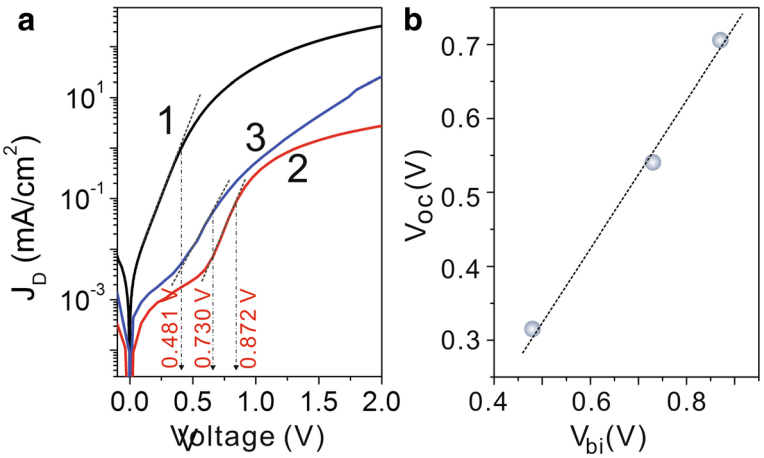

Fig. 6 **a** Semilogarithmic plots of dark J_D–V characteristics of devices based on TiO_2-NRA (*1*), TiO_2-NRA@TiO_2-QDs (*2*), and TiO_2-NRA@TiO_2-QDs@N719 (*3*). The *red dash lines* indicate V_{bi} values. **b** Dependence of V_{oc} on V_{bi} in devices

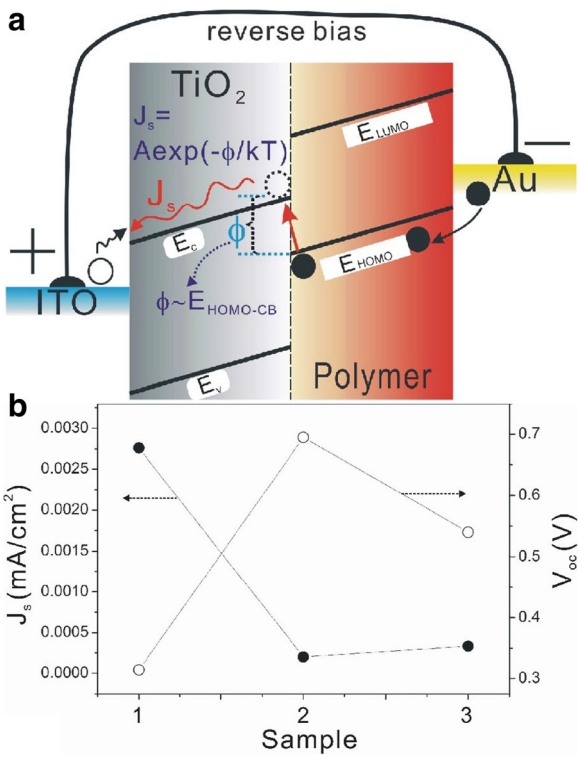

Fig. 7 **a** Illustration of the reverse bias current J_s and energetic barrier φ in polymer/TiO_2 HSCs. **b** Dependences of V_{oc} and J_S, in TiO_2-NRA- (*1*), TiO_2-NRA@TiO_2-QD- (*2*), and TiO_2-NRA@TiO_2-QDs@N719-based (*3*) solar cells. E_c and E_v indicate conduction and valence band of TiO_2, respectively; E_{LUMO} and E_{HOMO} indicate the highest occupied molecular orbital and lowest unoccupied molecular orbital of the polymer energy level, respectively

The current density–voltage of solar cells in the dark can be described by the following modified ideal diode equation [28]:

$$J_d = J_s\left(\exp\left(\frac{q(V-J_dR_s)}{nkT}\right)-1\right) \quad (3)$$

where J_s is reverse saturation current density, q elementary charge, V applied voltage, R_s device series resistance, n diode ideality factor, k Boltzmann's constant, and T temperature. We note that $V >> J_dR_s$ for our devices, since J_d generally less than 0.01 A/cm^2, and R_s is generally less than 200 Ω/cm^2. Neglecting the J_dR_s term in eq. (1), for $V \geq nkT/q$, we can get the following relation:

$$\ln J_d \approx \ln J_s + \frac{q}{nkT}V \quad (4)$$

Equation (4) indicates that a plot of $\ln J_d$ versus V should yield a straight line. Therefore, J_s and n can be extracted from the $\ln J_d$–V curves in the linear region, which q/nkT and $\ln J_s$ corresponds to the slope and y-intercept, respectively (Fig. 8). Therefore, we extracted the approximate value of dark reverse saturation current J_s from the dark J–V curve based on eq. 4 [29].

Based on eq. 2, we calculated the interface energy barrier Φ_B values of all devices (Fig.7b). The energy barrier ϕ for this process is correlated, but not necessarily just equal, to the difference between the E_c and E_{HOMO} (E_c–E_{Homo} in Fig. 7a) due to the complicated interfacial dynamic processes [28, 30]. If there was a shift of the E_c edge in the TiO_2 nanorod, it would affect the E_c–E_{Homo} (i.e., ϕ), and thereby influence the J_s, based on eq. 2. The changes of device J_s and V_{oc} with interfacial engineering are depicted in Fig. 7b. It is observed that J_s decreased from 2.76×10^{-3} mA/cm^2 in the MEH-PPV/TiO_2-NRA device to 2.03 ×

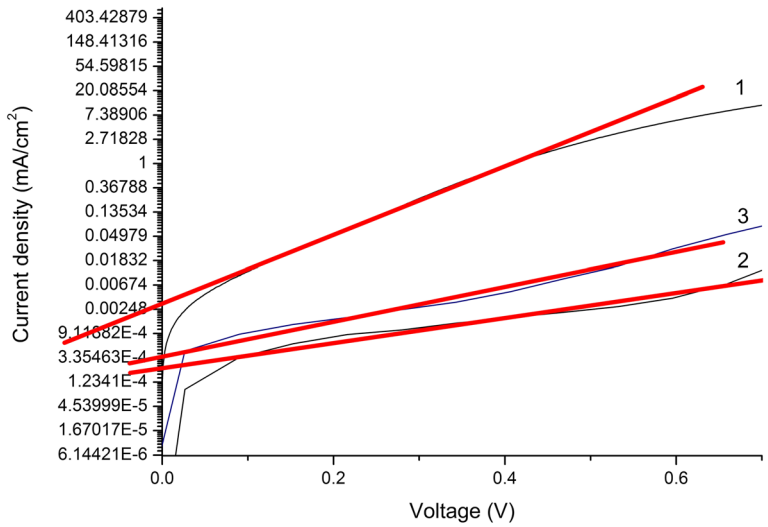

Fig. 8 $\ln J_d$–V curves of solar cells measured in the dark (TiO_2-NRA- (1), TiO_2-NRA@TiO_2-QD- (2), and TiO_2-NRA@TiO_2-QDs@N719-based (3))

10^{-4} mA/cm^2 in the MEH-PPV/TiO_2-NRA@TiO_2-QD device; therefore, the energy barrier ϕ (or E_c–E_{Homo}) increased based on eq. 2, which agrees with the expectation on the up-shift of the E_c edge in the TiO_2 nanorod after the growth of the QD layer in Fig. 5b. Additionally, the little increase of J_s (3.35×10^{-4} mA/cm^2) after the engineering of N719 agrees with the small downshift of the E_c edge in the TiO_2 nanorod (i.e., ϕ) due to the adsorbed N719 molecules on the TiO_2-QD surface with monodentate anchoring mode directed to the TiO_2 surface in Fig. 5b.

The improved J_{sc} in device performance after the interface modification was studied by IPCE and PL spectra (Fig. 9). The slightly enhanced IPCE (or J_{sc}) in the MEH-PPV/TiO_2-NRA@TiO_2-QD device resulted from the small increase of the interfacial area due to the formation of the coarse shell for exciton dissociation in comparison to the smooth surface of the original TiO_2 nanorods. However, the largely improved J_{sc} by modification of the TiO_2-NRA@TiO_2-QDs with N719 originates from the enhanced charge separation efficiency [22]. The amphiphilic dye improved the interface contact between the polymer and TiO_2-NRA@-TiO_2-QDs, which improves the electronic coupling property for charge transfer. These explanations agree with the PL quenching results (Fig. 9b). Obviously, the PL intensity of the MEH-PPV/TiO_2-NRA composite decreases significantly as compared with the intensity of pristine MEH-PPV, indicating that the PL emission of MEH-PPV can be quenched by TiO_2 nanorods resulting from the electron transfer from MEH-PPV to TiO_2 [31]. After engineering the TiO_2-NRA surface with TiO_2-QDs and TiO_2-QDs@N719, the degree of PL quenching become more obviously, especially in the MEH-PPV/TiO_2-NRA@TiO_2-QDs@N719 sample. The

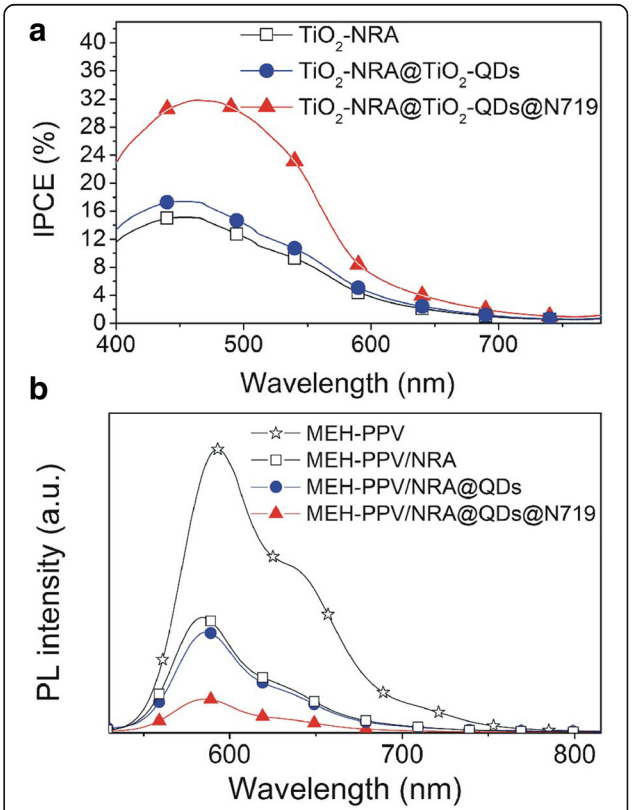

Fig. 9 a IPCE spectra of solar cells based on TiO_2-NRA, TiO_2-NRA@TiO_2-QD, and TiO_2-NRA@TiO_2-QD@N719 samples. **b** Room temperature PL spectra of the MEH-PPV and its composites with TiO_2-NRA, TiO_2-NRA@-TiO_2-QD, and TiO_2-NRA@TiO_2-QD@N719 samples

PL quenching and IPCE (or J_{sc}) follow similar trends indicating that the increased photocurrent upon the MEH-PPV/TiO_2-NRA@TiO_2-QDs@N719 indeed originates from the better charge separation and transfer at the heterojunction interface.

Conclusions

The heterojunction interfacial engineering in polymer/TiO_2 nanorod array (NRA) hybrid solar cells was performed in two steps: first, we grew TiO_2-quantum dots (QDs) on a TiO_2-NRA surface to form the TiO_2-NRA@-TiO_2-QD structure. Next, the TiO_2-NRA@TiO_2-QD structure was further bonded with organic molecules (N719) on its surfaces to form the TiO_2-NRA@TiO_2-QDs@N719 composite array through the solvothermal method. By controlling the interfacial engineering for polymer/TiO_2-NRA solar cells through the integration of TiO_2-QDs and N719 molecules, the V_{oc} and J_{sc} in polymer/TiO_2-NRA@TiO_2-QDs@N719 solar cells can be tuned, improving the device efficiency nearly four times compared with that of pristine TiO_2-NRA-based solar cells. The tunable device performance is resulted from the balanced interfacial dipoles, which is confirmed by the changed built-in voltage V_{bi} and reverse current J_s. These results therefore provide information crucial to the optimization of interface in HSCs.

Additional file

Additional file 1: Supplementary Data. Figure S1. XRD of TiO_2-NRA and TiO_2-NRA@TiO_2-QDs on the FTO substrate. Figure S2. (a) UV-vis absorption spectra of TiO_2-NRA (□), TiO_2-NRA@TiO_2-QDs (○), and TiO_2-NRA@TiO_2-QDs@N719 (△). The inset in (a) is the absorption spectra of N719 in the ethanol solution; (b) FT-IR spectra of TiO_2-NRA@TiO_2-QDs (1), TiO_2-NRA@-TiO_2-QDs@N719 (2), N719 (3). Figure S3. The *J*–*V* performance of fresh device and measured after 60 days. (DOC 4431 kb)

Acknowledgements
We acknowledge the "1112 Talents Project" of Huzhou City and the valuable suggestions from the peer reviewers.

Funding
The role of the National Natural Science Foundation of China (21607041; 11547312; 11647306) is designing the work; the role of the Zhejiang Provincial Natural Science Foundation of China (LQ14F040003) is purchasing the materials; and the role of the Science and Technology Planning Project of Zhejiang Province (2017C33240), Seed Fund of Young Scientific Research Talents of Huzhou University (RK21056), and Foundation of Science and Technology Innovation Activities & Emerging Talents Plan of Zhejiang Province (2015R427005; 2016R42707) is the collection, analysis, and interpretation of the data.

Authors' Contributions
FW carried out the experiments and drafted the manuscript. YZ, XY, and JX participated in the device preparation. XL participated in the design of the study. YT conceived of the study and helped to draft the manuscript. All authors read and approved the final manuscript.

Competing Interests
The authors declare that they have no competing interests.

Author details
[1]School of Science and Key Lab of Optoelectronic Materials and Devices, Huzhou University, Huzhou 313000, People's Republic of China. [2]Department of Material Chemistry, Huzhou University, Huzhou 313000, People's Republic of China.

Received: 12 October 2016 Accepted: 28 January 2017
Published online: 03 February 2017

References
1. Zheng L, Han S, Liu H, Yu P, Fang X (2016) Hierarchical MoS_2 nanosheet@TiO_2 nanotube array composites with enhanced photocatalytic and photocurrent performances. Small 12:1527–1536
2. Iandolo B, Wickman B, Svensson E, Paulsson D, Hellman A (2016) Tailoring charge recombination in photoelectrodes using oxide nanostructures. Nano Lett 16:2381–2386
3. Chiang C, Lee Y, Lee Y, Lin G, Yang M, Wang L, Hsieh C, Dai C (2016) One-step in situ hydrothermal fabrication of D/A poly(3-hexylthiophene)/TiO_2 hybridnanowires and its application in photovoltaic devices. J Mater Chem A 4:908–919
4. Armstrong CL, Price MB, Munoz-Rojas D, Davis NJKL, Abdi-Jalebi M, Friend RH, Greenham NC, MacManus-Driscoll JL, Böhm ML, Musselman KP (2015) Influence of an inorganic inter layer on exciton separation in hybrid solar cells. ACS Nano 9:11863–11871
5. Yu M, Long Y, Sun B, Fan Z (2012) Recent advances in solar cells based on one-dimensional nanostructure arrays. Nanoscale 4:2783–2796
6. Xu T, Qiao Q (2011) Conjugated polymer-inorganic semiconductor hybrid solar cells. Energy Environ Sci 4:2700
7. Xie YL (2013) Enhanced photovoltaic performance of hybrid solar cell using highly oriented CdS/CdSe-modified TiO_2 nanorods. Electrochim Acta 105: 137–141
8. Zhang Q, Yodyingyong S, Xi J, Myers D, Cao G (2012) Oxide nanowires for solar cell applications. Nanoscale 4:1436–1445
9. Liao W, Hsu S, Lin W, Wu J (2012) Hierarchical TiO_2 nanostructured array/P3HT hybrid solar cells with interfacial modification. J Phys Chem C 116: 15938–15945
10. Baeten L, Conings B, D'Haen J, Hardy A, Manca JV, Van Bael MK (2012) Fully water-processable metal oxide nanorods/polymer hybrid solar cells. Sol Energy Mater Sol Cells 107:230–235
11. Hsu S, Liao W, Lin W, Wu J (2012) Modulation of photocarrier dynamics in indoline dye-modified TiO_2 nanorod array/P3HT hybrid solar cell with 4-tert-butylpyridine. J Phys Chem C 116:25721–25726
12. Liao W, Wu J (2013) Efficient electron collection in hybrid polymer solar cells: in-situ-generated ZnO/poly(3-hexylthiophene) scaffolded by a TiO_2 nanorod array. J Phys Chem Lett 4:1983–1988
13. Lu H, Joy J, Gaspar RL, Bradforth SE, Brutchey L (2016) Iodide-passivated colloidal PbS nanocrystals leading to highly efficient polymer: nanocrystal hybrid solar cells. Chem Mater 28:1897–1906
14. Wang J, Zhang T, Wang D, Pan R, Wang Q, Xia H (2012) Influence of CdSe quantum dot interlayer on the performance of polymer/TiO_2 nanorod arrays hybrid solar cell. Chem Phys Lett 541:105–109
15. Xia H, Zhang T, Wang D, Wang J, Liang K (2013) Composite interfacial modification in TiO2 nanorod array/poly (3-hexylthiophene) hybrid photovoltaic devices. J Alloys Compd 575:218–222
16. Liu B, Aydil ES (2009) Growth of oriented single-crystalline rutile TiO_2 nanorods on transparent conducting substrates for dye-sensitized solar cells. J Am Chem Soc 131:3985
17. Wu F, Chen C, Zhao Y, Zhang H, Li X, Lu W, Zhang T (2014) Changes of V_{oc} in hybrid solar cells by TiO_2 nanoarray with different crystallinity of shell. J Electrochem Soc 161:H593–H597
18. Wu F, Cui Q, Qiu Z, Liu C, Zhang H, Shen W, Wang M (2013) Improved open-circuit voltage in polymer/oxide-nanoarray hybrid solar cells by formation of homogeneous metal oxide core/shell structures. ACS Appl Mater Interfaces 5:3246–3254
19. Ramsdale CM, Barker JA, Arias AC, MacKenzie JD, Friend RH, Greenham NC (2002) The origin of the open-circuit voltage in polyfluorene-based photovoltaic devices. J Appl Phys 92:4266–4270
20. Tan ZK, Johnson K, Vaynzof Y, Bakulin AA, Chua LL, Ho PKH, Friend RH (2013) Suppressing recombination in polymer photovoltaic devices via energy-level cascades. Adv Mater 25:4131–4138

21. Goh C, Scully SR, McGehee MD (2007) Effects of molecular interface modification in hybrid organic-inorganic photovoltaic cells. J Appl Phys 101:114503
22. Ruankham P, Macaraig L, Sagawa T, Nakazumi H, Yoshikawa S (2011) Surface modification of ZnO nanorods with small organic molecular dyes for polymer-inorganic hybrid solar cells. J Phys Chem C 115:23809–23816
23. Krüger J, Bach U, Grätzel M (2000) Modification of TiO_2 heterojunctions with benzoic acid derivatives in hybrid molecular solid-state devices. Adv Mater 12:447–451
24. Samadpour M, Irajizad A, Taghavinia N, Molaei M (2011) A new structure to increase the photostability of CdTe quantum dot sensitized solar cells. J Phys D Appl Phys 44:045103
25. Mihailetchi VD, Blom PWM, Hummelen JC, Rispens MT (2003) Cathode dependence of the open-circuit voltage of polymer: fullerene bulk heterojunction solar cells. J Appl Phys 94:6849
26. Kippelen B, Brédas JL (2009) Organic photovoltaics. Energy Environ Sci 2:251
27. Potscavage WJ, Yoo S, Kippelen B (2008) Origin of the open-circuit voltage in multilayer heterojunction organic solar cells. Appl Phys Lett 93:193308
28. Stevens DM, Speros JC, Hillmyer MA, Frisbie CD (2011) Relationship between diode saturation current and open circuit voltage in poly(3-alkylthiophene) solar cells as a function of device architecture, processing conditions, and alkyl side chain length. J Phys Chem C 115:20806
29. Lee YJ, Davis RJ, Lloyd MT, Provencio PP, Prasankumar RP, Hsu JWP (2010) Open-circuit voltage improvement in hybrid ZnO–polymer photovoltaic devices with oxide engineering. IEEE J Sel Top Quantum Electron 16:1587–1594
30. Siddiki MK, Venkatesan S, Galipeau D, Qiao Q (2013) Kelvin probe force microscopic imaging of the energy barrier and energetically favorable offset of interfaces in double-junction organic solar cells. ACS Appl Mater Interfaces 5:1279–1286
31. Ton-That C, Stockton G, Phillips MR, Nguyen TP, Huang CH, Cojocaru A (2008) Luminescence properties of poly-(phenylene vinylene) derivatives. Polym Int 57:496–501